ACADEMIC PRESS

Available online at www.sciencedirect.com

SCIENCE DIRECT®

Journal of Sound and Vibration 271 (2004) 103–130

JOURNAL OF SOUND AND VIBRATION

www.elsevier.com/locate/jsvi

Studies on dynamic behavior of composite and isotropic cylindrical shells with PZT layers under axisymmetric temperature variation

Ravikiran Kadoli, N. Ganesan*

Machine Dynamics Laboratory, Department of Applied Mechanics, Indian Institute of Technology, Chennai 600036, India

Received 24 September 2002; accepted 28 February 2003

Abstract

A comparative study is presented on the vibratory characteristics of isotropic and orthotropic cylindrical shells with perfectly bonded piezoelectric material on the inner and outer surface of the shell lamina. The variation of free vibration natural frequencies and active damping ratios are simulated under varying magnitude of steady state axisymmetric temperatures. The objectives are explained by presenting the results of the numerical study on cylindrical shells made of mild steel and HS-graphite/epoxy bonded with PZT piezoelectric material. The vibratory characteristics under the above circumstances are interpreted from the point of view of initial stresses developed due to thermal loading. Apart from this, the changes in the vibratory characteristics due to different fiber orientations are examined. It is found from the studies that the frequency characteristic with respect to fiber orientation under thermal environment is highly dependent on the boundary condition considered for the shell laminate.

1. Introduction

Structural components in many application are exposed to temperature gradients as well as to vibrations as in spacecraft, high-speed aircraft, manipulators in heat treatment shops to quote a few. Knowledge of natural frequency and buckling analyses under thermal loading are critical components of a design. Inherent vibration modes in structural components or mechanical support systems can shorten equipment life and cause unexpected failures. The role of the thermal component and its influence during the control of vibration amplitude using piezoelectric material is becoming necessary. Most of the active vibration control research is directed towards

*Corresponding author. Tel.: +91-44-2351365; fax: +91-44-2350509.
E-mail address: nganesan@iitm.ac.in (N. Ganesan).

0022-460X/03/$ - see front matter
doi:10.1016/S0022-460X(03)00265-7

understanding the behavior of piezoelectric material bonded (or embedded) on laminated components when simultaneously subjected to mechanical, electric and temperature loadings, commonly referred to as piezothermoelastic behavior. Useful research is reported on isotropic as well as orthotropic beams, plates and shells. Recently Tauchert et al. [1] have reviewed the state of the art research reported in the area of piezothermoelasticity in smart composite structures. They provide brief information regarding the equations governing piezothermoelastic response, general solution procedure for piezothermoelastic bodies, piezoelectric sensor applications and control of composite structures like laminated beams, plates and shells via piezoelectric actuation. Rao and Sunar [2] have made a deep survey of the research work reported on distributed sensing and control of flexible structures using piezoelectricity. In their work, Rao and Sunar [3] were able to show how important it is to include thermal effects in the application of distributed dynamic measurement and active vibration control of advanced intelligent structures with illustrations on a flexible bimorph robotic finger working in temperature changing environment.

Many researchers have produced results of their studies on the exact solutions for piezoelectric shells for various loading conditions like pressure, thermal and electric potential. Chen and Shen [4] carried out analytical studies on orthotropic circular cylindrical shell laminate with piezoelectric layer subjected to axisymmetric thermal and mechanical loadings. Xu and Noor [5] obtained analytical three-dimensional solutions for the thermoelectroelastic response of hybrid laminated cylindrical shells. The solutions presented provide physical insight into the interaction between the mechanical, thermal, and electric fields. Kapuria et al. [6–9] have worked extensively in obtaining exact solutions for piezothermoelastic cylindrical shells and hybrid shell laminates under axisymmetric and non-axisymmetric loadings. For example, under axisymmetric loading, solutions are presented for finite transversely isotropic axially polarized piezoelectric cylindrical shell [6], three dimensional series solution for a simply supported piezoelectric circular cylindrical shell (PVDF) [7], hybrid cylindrical shell made of graphite-epoxy composite laminate and bonded by PVDF layers [8] and for non-axisymmetric pressure load, thermal load and applied potential, obtained an exact three-dimensional solution for a cylindrical hybrid composite shell with surfaces bonded with PZT-5a [9]. In all these studies the variations of displacements, stresses, electric potential and electric displacement across the thickness of the piezoelectric shell or hybrid shell laminate were examined for various ratios of radius to thickness and loading patterns. Also in the case of hybrid shell laminate they illustrated that the maximum values of deflection and the stresses due to thermal loading developed in the composite laminate and PVDF layers could be reduced considerably by applying actuation potential to the piezoelectric layer. The three-dimensional analysis of piezothermoelastic behavior under different loading cases as studied by above authors Chen and Shen, Xu and Noor, and Kapuria et al. will be helpful in assessing the one- and two-dimensional piezothermoelastic models. Fung et al. [10] investigated the dynamic behavior of a piezothermoelastic resonator cantilever beam of various shapes with variations like stepped, linearly tapered and exponential. The steady state temperature rise distribution caused by the actuation of applied voltage was calculated and its effects on the behavior of the resonator were studied. Professor H.S. Tzou along with his co-researchers have been contributing enormous amount of literature related to piezothermoelastic behavior. Tzou and Bao [11] have developed a theory to study the behavior of anisotropic piezothermoelastic shell laminates involving piezoelectric materials. Using Hamilton's principle thermo-electromechanical equations and boundary conditions of arbitrary anisotropic piezoelectric shell laminates were derived. Further

they illustrate the use of the theory to obtain governing equations for cases like laminated shell made of PVDF and for a single layer PVDF shell experiencing temperature variations. Tzou and Howard [12] derived a generic piezothermoelastic shell theory for thin piezoelectric shells based on linear piezoelectric theory and Kirchoff–Love assumptions. The theory can be used for the analysis of piezoelectric cylindrical shell, piezoelectric ring, beam etc. by changing the Lame's parameters and radii of curvatures. Thermal effects to sensing and control of active piezoelectric structures are discussed. Tzou and Ye [13] have developed a thin piezothermoelastic solid finite element based on the variational formulation for piezothermoelasticity. The capability of the piezothermoelastic finite element model is illustrated by studying the dynamic response of free and controlled vibrations of the PZT laminated steel beam with and without thermal excitation. They indicate in their study that there exists thermal deflection over the dynamic oscillation. In order to control simultaneously the dynamic oscillation as well as thermal-induced deflection, two control voltages are required. Tzou and Bao [14] have formulated the theoretical background for the analysis of non-linear piezothermoelastic characteristics of anisotropic piezoelectric laminated shells undergoing large deformations (i.e. geometric non-linearities). The mathematical model is general in nature and one can appropriately deduce from this model to study and analyze non-linear piezothermoelastic behavior and active static and dynamic control of plates, shells of revolution etc. In continuation to this publication by Tzou and Bao, Tzou and Zhou [15] implemented the non-linear piezothermoelastic theory to study the control of non-linear deflection, buckling and dynamics of piezoelectric laminated circular plate. The laminated circular plate experiences large non-linear deformation and is subjected to mechanical, temperature and electric excitations. Lee and Saravanos [16] have constructed analytical formulations to study the response from a piezoelectric composite shell structures under the coupled mechanical loading, electric loading and thermal loading. Derived finite element equations and implemented for an eight-node shell element, conducted investigations on the sensory and active responses of piezoelectric composite shell structures subjected to thermal loads and also demonstrated the thermal shape control of a cylindrical shell on to which is bonded piezoelectric layer. Gu et al. [17] addresses bi-way coupling effects between temperature, piezoelectric and mechanical fields in the study of smart composites and active control techniques in the presence of temperature fields. A new higher order temperature field is developed in order to determine the temperature field through the plate thickness. Refined third order displacement field is used to determine the transverse shear. A finite element technique is developed based on these theories to study the response of composite laminated plate with surface bonded PZT actuators and sensors.

There exists another class of materials developed from a combination of two materials with varying proportion over the thickness so as to take advantage of their best and suitable material properties and these are referred to as functionally graded materials (FGM). The most familiar FGM is compositionally graded from a refractory ceramic to a metal (steel or aluminum). It can incorporate incompatible functions such as the heat, wear, and oxidation resistance of ceramics and the high toughness, high strength, machinability and bonding capability of metals without severe internal thermal stress. These materials are proposed to be suitable for aerospace structural components, components for combustion chamber construction and in areas where one encounters large temperature variations. Active control studies on the FGM components are building up rapidly in the repertoire of engineering and technology's literature. He et al. [18] developed a finite element model based on classical laminated plate theory for the analysis of

static displacement control and vibration control of FGM plates with piezoelectric sensors and actuators. They illustrate the control of center line deflection for a clamped–free–free–free FGM plate under uniformly distributed load for various actuator voltages and power law exponents, which dictates the properties variation through the thickness. For vibration suppression analysis of FGM plate, the transient response was obtained using Newmark-β direct integration scheme. Liew et al. [19] have conducted piezothermoelastic analysis of FGM plates. They developed a finite element formulation for the same based on first order shear deformation theory. The FGM plate is exposed to a temperature gradient through the thickness. A constant displacement feedback control is used to minimize the bending deflection of the plate. Bending and torsional vibration were controlled using a constant displacement cum velocity feedback. Influence of various volume fraction exponent and controller gain values were examined. He et al. [20] carried out studies on active control of curved FGM shells. The finite element model for the analysis of piezoelectric layered FGM curved shell is developed based on the Kirchoff–Love theory and linear piezoelectric theory. Using a displacement-cum-velocity feedback controller to couple the piezoelectric sensors and actuators to form a close loop active control system, simulation studies were presented on static and dynamic control of FGM shell laminates. The influence of various values of volume fraction exponent and controller gains was also examined. Ng et al. [21] have carried out studies on the dynamic stability of FGM plates under harmonic in-plane loading. Dynamic instability regions are evaluated for simply supported FGM plates for different values of power law exponent and for different loading configuration. Their studies reveal that, to some extent it is possible to control the origin of the unstable point by varying the volume fraction exponent. Parametric resonance of simply supported FGM cylindrical shells under periodic axial loading was studied by Ng et al. [22]. A second order differential equation with periodic coefficients of the Mathieu-Hill type is derived. The Bolotin's first approximation is used to evaluate the periodic solution. They report that the natural frequencies and dynamic instability regions can be fairly controlled by appropriately varying the power law exponent. Recently Ng et al. [23] developed an efficient finite element formulation based on the first order shear deformation theory for active control of FGM shells in the frequency domain. They illustrated the application of their formulation for a cantilever FGM shell with piezoelectric sensor and actuator layers and subjected to a harmonic excitation. Natural frequencies can be controlled to desired values by adjusting the displacement control gain or the volume fraction of the constituent materials. Vibration amplitudes can be controlled by increasing the damping via displacement velocity feedback gain.

Recently, the present authors [24] have reported their studies on the buckling and dynamic behavior of piezothermoelastic composite cylindrical shell with clamped–clamped boundary condition. Exhaustive results are reported on how the fiber angles of composite lamina can influence the limiting value of thermal buckling temperature. Also the influence of number of plies, the material properties like Young's modulus and coefficient of thermal expansion on the thermal buckling temperatures were examined. The influence of temperature on the natural frequency has been studied for two typical cases and damping results have been presented for a typical case. In contrast the main aim of the present study is to compare the behavior of simply supported and clamped–free PZT layered orthotropic and isotropic cylindrical shell for dynamic behavior and mention clearly the influence of boundary condition. In addition further study is made to compare the behavior of composite shells in relation to isotropic shells.

This paper focuses on the study of vibration characteristics of PZT layered cylindrical shell made of mild steel and HS-graphite/epoxy material under steady state temperature conditions. The PZT layer is fully distributed over the inner and outer surface of the cylindrical shell. The PZT layers are specially shaped to a cosine form so that potential variation can be expressed in Fourier series. Based on the linear piezothermoelastic constitutive equations an uncoupled electromechanical and thermomechanical analysis is undertaken. An in depth comparative aspects related to free vibration natural frequency characteristics, static thermal buckling temperature, frequency behavior for various axisymmetric temperature and active damping ratio have been dealt. Since composites can be tailored to any required fiber angle, for a single layered cylindrical shell various fiber angles are considered. As a result of this a detailed comparison is being spelt out in regards to composite shell with various fiber angles and mild steel (isotropic) material. This will bring out the best possible fiber angle for HS-graphite/epoxy composite material when compared to mild steel (conventional isotropic) material. Further the role of the boundary condition on the overall characteristics in also examined. It is found that composite material with certain fiber angle for the lamina can give superior thermal buckling temperature and hence vibration characteristics when compared to isotropic material. Numerical results have been obtained by considering cylindrical shell with $l/r = 2.08$ and $r/h = 292.0$. Boundary conditions considered are simply supported at both ends and clamped–free. Isothermal conditions are assumed to exist with the temperature variation as axisymmetric in nature. The numerical analysis is carried out using a semi-analytical finite element formulation worked out for laminated shells of revolution comprising of piezoceramic layers bonded to isotropic or composite shell. The structural finite element formulation is adopted from the work of Rao et al. [25]. The active control strategy based on cosine shaped PZT sensor/actuators with negative velocity feedback control as developed by Saravanan et al. [26] is used. The semi-analytical formulation to consider the temperature effects for shells of revolution is developed and appended to the above two formulations. The initial stresses due to thermal loading can be determined and hence the geometric stiffness matrix evaluated. The semi-analytical finite element code developed for the study of thermal effects in PZT bonded cylindrical shell is independently validated for thermal buckling temperatures, and the results are found to agree well with the available literature.

2. The physical model

The piezothermoelastic continua comprises of a cylindrical shell of length l, mid-surface radius r, and thickness h. The outer and inner surface of the shell is perfectly bonded with piezoceramic material. These distributed sensors and actuators are of the convolving type, $\cos k\theta$ shaped, similar to that proposed by Tzou et al. [27]. The sensor signals are modified by a negative velocity feedback controller with a constant gain and supplied to the actuators. The system comprising of the piezoceramic bonded cylindrical shell is exposed to steady state heat source $\mathbf{q}$ such that steady state heat influx q_{si} into the system equals the steady state heat dissipated q_{so} from the system. The system operates under steady state temperature and temperature variation through the continua is axisymmetric. The continua are modelled in tri-orthogonal curvilinear co-ordinate system (s, θ, z) as shown in Fig. 1.

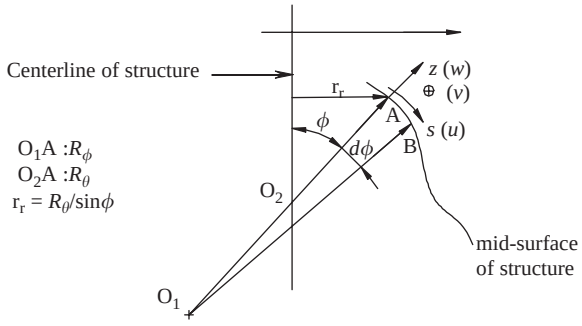

Fig. 1. Orthogonal curvilinear co-ordinate system for shells of revolution.

The three fundamental equations of the piezothermoelastic constitutive relations are the stress equation (Duhamel–Neumann equation), the electric displacement equation and entropy density equation are expressed using notation of Mindlin [28] are written as follows:

$$\sigma_{ij} = c_{ijkl}(\varepsilon_{kl} - \varepsilon^o_{kl}) - e_{kij}E_k - \lambda_{ij}T, \tag{1}$$

$$D_i = e_{ikl}(\varepsilon_{kl} - \varepsilon^o_{kl}) + \xi_{ik}E_k + p_i T, \tag{2}$$

$$\eta = \lambda_{kl}(\varepsilon_{kl} - \varepsilon^o_{kl}) + p_k E_k + \frac{\rho c_v}{T_o}, \tag{3}$$

where σ_{ij} is the stress tensor, c_{ijkl} is the elastic coefficients at the constant electric field and temperature, ε_{kl} is the strain tensor, ε^o_{kl} is the initial strain vector, e_{ijk} is the piezoelectric coefficients at a constant temperature, E_k is the electric field, λ_{ij} is the temperature-stress coefficient, T is the temperature rise from stress free reference temperature T_o. D_i is the electric displacement component, ξ_{ik} is the dielectric coefficient at the constant elastic stress and temperature, p_i is the pyroelectric constant, η is the entropy per unit volume, c_v is the specific heat at constant volume and ρ is the density of the material. The formulation to follow in the subsequent sections does not take into account the electromechanical and thermomechanical coupling.

3. Semi-analytical finite element method for analysis of piezothermoelastic behavior of PZT bonded shells of revolution

3.1. Structural stiffness and mass matrix

Liew [29] has recently provided an elaborate review on the vibration studies carried out on thin, moderately thick, and thick shallow shells. Even though exhaustive reviews are available in the literature, Liew lays more stress on aspects of vibration studies of shells using shell theories which account for transverse shear effects. The displacement field on the basis of first order shear deformation theory of the structural continuum is referred with respect to curvilinear co-ordinate system (s, θ, z). The total displacement is expressed as a sum of the mid-surface displacements u_o, v_o, w_o along the s, θ, and z directions and rotations of the normal to the mid-surface ψ_s, ψ_θ along s

and θ axes respectively, which can be written in a matrix form

$$\{\mathbf{f}\}=[\mathbf{H}]\{\mathbf{f_o}\}, \tag{4}$$

where

$$\{\mathbf{f_o}\}^{\mathrm{T}} = [\,u_o \quad v_o \quad w_o \quad \psi_s \quad \psi_\theta\,], \quad [H] = \begin{bmatrix} 1 & 0 & 0 & z & 0 \\ 0 & 1 & 0 & 0 & z \\ 0 & 0 & 1 & 0 & 0 \end{bmatrix} \text{ and } \{\mathbf{f}\}^{\mathrm{T}} = \{\,u \quad v \quad w\,\}.$$

In the semi-analytical approach, the generalized displacement field is assumed to depend in the circumferential direction and is expanded in Fourier series in the θ direction as follows:

$$u_o = \sum_{m=0}^{\infty} u_{om}\cos m\theta, \qquad v_o = \sum_{m=0}^{\infty} v_{om}\sin m\theta, \qquad w_o = \sum_{m=0}^{\infty} w_{om}\cos m\theta,$$
$$\psi_{os} = \sum_{m=0}^{\infty} \psi_{osm}\cos m\theta, \quad \psi_{o\theta} = \sum_{m=3}^{\infty} \psi_{o\theta m}\sin m\theta.$$

Various Fourier harmonics would be decoupled if one considers only small vibrations. The displacement field in Eq. (4) along with the strain–displacement relations for a doubly curved shell of revolution in the (s,θ,z) co-ordinate as given in Rao and Ganesan [25] based on FSDT and elasticity theory will provide the following kinematic relations.

$$\varepsilon_{ss} = \frac{1}{A_1}(\varepsilon^o_{ss} + z\kappa^1_s), \quad \gamma_{\theta z} = \frac{1}{A_2}\gamma^o_{\theta z}, \tag{5a, 5b}$$

$$\varepsilon_{\theta\theta} = \frac{1}{A_2}(\varepsilon^o_{\theta\theta} + z\kappa^1_\theta), \quad \gamma_{sz} = \frac{1}{A_1}\gamma^o_{sz}, \tag{5c, 5d}$$

$$\gamma_{s\theta} = \frac{1}{A_1}\frac{1}{A_2}(\gamma^o_{s\theta} + z\kappa^1_{s\theta}), \tag{5e, 5f}$$

where

$$\frac{1}{A_1} = \frac{1}{(1+z/R_\phi)} \text{ and } \frac{1}{A_2} = \frac{1}{(1+z/R_\theta)}$$

In the above equations R_ϕ and R_θ are the principle radii of curvature of the shell as illustrated in Fig. 1. Based on the magnitudes of R_ϕ and R_θ the geometry of the shell can become a cylindrical shell, conical shell or a spherical shell. $\varepsilon_{ss}, \varepsilon_{\theta\theta}, \gamma_{\theta z}, \gamma_{sz}, \gamma_{s\theta}$ are the total strains which comprise of normal strains and the shear strains: $\varepsilon^o_{ss}, \varepsilon^o_{\theta\theta}, \gamma^o_{\theta z}, \gamma^o_{sz}, \gamma^o_{s\theta}$ referred to mid-surface and $\kappa^1_s, \kappa^1_\theta, \kappa^1_{s\theta}$, are the change in curvature.

The total strain energy in the laminated cylindrical shell is given by

$$U = U_1 + U_2,$$

where U_1 is the strain energy due to vibratory stresses and U_2 is the strain energy due to initial stresses as a result of steady state temperature. Strain energy U_1 is given by

$$U_1 = \frac{1}{2}\int_V \{\varepsilon_{ss}\sigma_{ss} + \varepsilon_{\theta\theta}\sigma_{\theta\theta} + \gamma_{\theta z}\tau_{\theta z} + \gamma_{sz}\tau_{sz} + \gamma_{s\theta}\tau_{s\theta}\}\,\mathrm{d}V,$$

$$U_1 = \frac{1}{2}\int \{\boldsymbol{\varepsilon}\}^{\mathrm{T}}\{\boldsymbol{\sigma}\}\,\mathrm{d}A, \tag{6}$$

where $\{\boldsymbol{\sigma}\}$ and $\{\boldsymbol{\varepsilon}\}$ are the generalized stress and strain vectors, respectively, and $\mathrm{d}A$ is the infinitesimal area element on the shell mid-surface. The foregoing vectors are defined by

$$\{\boldsymbol{\varepsilon}\}^{\mathrm{T}} = \{\varepsilon_{ss}^{o}\varepsilon_{\theta\theta}^{o}\gamma_{s\theta}^{o}\kappa_{s}^{1}\kappa_{\theta}^{1}\kappa_{s\theta}^{1}\gamma_{sz}^{o}\gamma_{\theta z}^{o}\},$$

$$\{\boldsymbol{\sigma}\}^{\mathrm{T}} = \{N_{ss}N_{\theta\theta}N_{s\theta}M_{ss}M_{\theta\theta}M_{s\theta}Q_{s}Q_{\theta}\}.$$

The methodology for the derivation of the element stiffness matrix for the shell laminate is based on the usual finite element procedure.

The mass matrix is obtained from the kinetic energy of the shell continuum, $KE = \frac{\rho}{2}\int_{V}(\dot{u}^2 + \dot{v}^2 + \dot{w}^2)\,\mathrm{d}V$. For details see Ref. [24].

3.2. Geometric stiffness matrix evaluation

The PZT layered cylindrical shell is assumed to operate at a constant temperature. Thus there exists thermal deflection and hence initial stresses. Neglecting the strain energy due to initial transverse shear stresses, the expression for the strain energy due to initial stresses U_2 is stated in Rao [30] is as follows

$$\mathrm{U}_2 = \frac{1}{2}\int_{V}\{(\varepsilon_{ss}^{i})^2\sigma_{ss}^{*} + (\varepsilon_{\theta\theta}^{i})^2\sigma_{\theta\theta}^{*} + 2\gamma_{s\theta}^{i}\,\tau_{s\theta}^{*}\}\,\mathrm{d}V \tag{7}$$

in which $\sigma_{ss}^{*}, \sigma_{\theta\theta}^{*}$, and $\tau_{s\theta}^{*}$ are the initial stresses and the corresponding strains $\varepsilon_{ss}^{i}, \varepsilon_{\theta\theta}^{i}$ and $\gamma_{s\theta}^{i}$ are given as follows

$$\varepsilon_{ss}^{i} = \frac{1}{(1 + z/R_{\phi})}\left(\frac{\partial w^{i}}{\partial s} - \frac{u^{i}}{R_{\phi}}\right), \tag{8}$$

$$\varepsilon_{\theta\theta}^{i} = \frac{1}{(1 + z/R_{\theta})}\left(\frac{1}{r}\frac{\partial w^{i}}{\partial \theta} - \frac{v^{i}}{r}\sin\phi\right). \tag{9}$$

$$\gamma_{s\theta}^{i} = \varepsilon_{ss}^{i}\varepsilon_{\theta\theta}^{i} \tag{10}$$

Using Eqs. (8)–(10) into Eq. (7) leads to

$$U_2 = \tfrac{1}{2}\{\mathbf{d}_{e}^{\mathrm{i}}\}^{\mathrm{T}}[\mathbf{k}_{\sigma e}]\{\mathbf{d}_{e}^{i}\}.$$

The matrix $[\mathbf{k}_{\sigma e}]$ in the foregoing equation is the element geometric stiffness matrix:

$$[\mathbf{k}_{\sigma e}] = \int_{V}[\mathbf{B}^{i}]^{\mathrm{T}}\{\boldsymbol{\sigma}^{*}\}\,\mathrm{d}V. \tag{11}$$

The strain displacement relation is given by $\{\boldsymbol{\varepsilon}^{i}\}=[\mathbf{B}^{i}]\{\mathbf{d}_{e}^{i}\}$ where $\{\mathbf{d}_{e}^{i}\}$ represents the elemental displacement vector. To compute the initial stresses due to axisymmetric temperature it is necessary to find the thermal load and hence the displacement vector due to constant temperature and the procedure is detailed in the next section.

3.3. Thermal load and initial stress evaluation

Under thermal environment the expression for the total potential for an element is as follows

$$\Pi = \frac{1}{2}\int_V \{\boldsymbol{\varepsilon}\}^{\mathrm{T}}[\mathbf{D}]\{\boldsymbol{\varepsilon}\}\,\mathrm{d}V - \int_V \{\boldsymbol{\varepsilon}\}^{\mathrm{T}}\{\boldsymbol{\lambda}\}T\,\mathrm{d}V. \tag{12}$$

The temperature is assumed to be constant over the thickness and the temperature field for the shell and piezoceramic continua is $T(s,\theta,z,t) = T(s,\theta,t)$. Steady state temperature is assumed to be dependent in the circumferential direction, and using Fourier series the temperature in the circumferential direction is

$$T = \sum_{m=0}^{\infty} T_m \cos m\theta.$$

Evaluation of the stress resultants has been detailed in the work published by Ganesan and Kadoli [24] which is similar to that described in Cook et al. [31]. In brief the procedure involved is (i) the computation of the thermal load vector, (ii) obtaining the thermal deflections, (iii) computing the mechanical stress resultants, and finally (iv) superposing the stress resultants due to temperature field.

3.4. Active control under steady state axisymmetric temperature field

The linear piezothermoelastic constitutive relations i.e. Eqs. (1) and (2), namely the converse piezoelectric and the direct piezoelectric effects will be used to obtain the finite element active damping matrix. The procedure outlined below is based on the theory developed for a distributed piezoelectric sensing by Tzou [32] and Tzou et al. [33]. The sensor and actuator equations will be developed separately.

$$\{\mathbf{E}\} = \{\, E_s \quad E_\theta \quad E_z \,\}^{\mathrm{T}}.$$

The piezoceramic sensor and actuator layers are very thin of the order of 0.02 mm. In the above equation the quantity corresponding to, E_θ, is assumed to have cosine distribution in the θ direction. In the present study the contribution of the potential in the θ direction is ignored. It should be borne in mind that ignoring this quantity may have a significant effect on the closed loop natural frequency. However, the present analysis considers the poling of electrodes in the transverse direction only. The potential φ in the piezoelectric layer is assumed to vary linearly over the thickness, hence

$$\{\mathbf{E}\} = \left\{ 0 \quad 0 \quad -\frac{\varphi}{t_p} \right\}^{\mathrm{T}},$$

where t_p is the thickness of the piezoceramic sensor layer. Referring to Tzou [34], in sensor application, it is assumed that electric displacement, D_i, is zero in an open circuit boundary condition. Hence using Eq. (2)

$$-\int_{A_s} [\boldsymbol{\xi}]\{\mathbf{E}\}\,\mathrm{d}A = \int_{A_s} [\mathbf{e}]\{\boldsymbol{\varepsilon}\}\,\mathrm{d}A + \int_A \{\mathbf{p}\}T\,\mathrm{d}A,$$

$$\varphi_s = -\frac{1}{\xi_{33}A_{elec}}\left(t_s \int_{A_{elec}} [\, e_{31} \quad e_{32} \,] \left\{ \begin{matrix} \varepsilon_{ss} \\ \varepsilon_{\theta\theta} \end{matrix} \right\} \mathrm{d}A + t_s \int_A \{p\}T\,\mathrm{d}A \right). \tag{13}$$

Note that Eq. (13) gives us the averaged charge and A_{elec} is the area of the electrode. The constitutive relation that defines the converse piezoelectric effect i.e. Eq. (1) is used to determine the actuating force generated by distributed actuators.

$$\sigma_{ij} = c_{ijkl}\varepsilon_{kl} - e_{kij}E_k - \lambda_{ij}T.$$

In the above equation the effects due to axisymmetric temperature are the initial stresses which are accounted in geometric stiffness matrix. Operating on other terms, from the principle of virtual work the actuating force is computed as follows

$$\{\delta\boldsymbol{\varepsilon}\}^{\mathrm{T}}\{\boldsymbol{\sigma}\} = \int_V \{\delta\boldsymbol{\varepsilon}\}^{\mathrm{T}}[D]\{\delta\boldsymbol{\varepsilon}\}\,\mathrm{d}V - \int_V \{\delta\boldsymbol{\varepsilon}\}^{\mathrm{T}}[\mathbf{e}]^{\mathrm{T}}\{\mathbf{E}\}\,\mathrm{d}V.$$

The effect of mechanical induced strain in the piezoceramic layer is neglected hence the actuator force will be

$$\{\mathbf{F}\} = [\mathbf{k}^a_{u\varphi}]\left(\frac{\varphi_a}{t_a}\right), \tag{14}$$

where φ_a is the actuator potential and t_a is the thickness of actuator. The negative velocity feedback controller is defined as

$$\varphi_a = -G_F\dot{\varphi}_s, \tag{15}$$

where $\dot{\varphi}_s$ is the time derivative of φ_s and G_F is the feedback factor. Substituting Eq. (13) after taking the time derivative into Eq. (15) the actuator potential will be

$$\varphi_a = G_F\frac{1}{\xi_{33}A_{elec}}\left(t_s\int_{A_{elec}}[\mathbf{e}][\mathbf{B}]\,\mathrm{d}A\{\dot{\mathbf{d}}\} + t_s\int_A\{p\}\dot{T}\,\mathrm{d}A\right). \tag{16}$$

Since the temperature is assumed to be steady the time derivative of temperature is zero accordingly substituting Eq. (16) in Eq. (14) the actuator force will now become

$$\{\mathbf{F}\} = [\mathbf{k}^a_{u\varphi}]\left(G_F\frac{1}{\xi_{33}A_{elec}}\left(\int_{A_{elec}}[\mathbf{e}][\mathbf{B}]\,\mathrm{d}A\{\dot{\mathbf{d}}\}\right)\right)$$

or

$$[\mathbf{c}_{ae}] = [\mathbf{k}^a_{u\varphi}]((G_F)[\mathbf{k}^s_{u\varphi}]). \tag{17}$$

The above equation represents the active damping matrix $[\mathbf{c}_{ae}]$ for an element.

4. Prebuckling analysis and equation of motion

The static thermal buckling solution is obtained for an arbitrary axisymmetric temperature distribution. The following equation is solved to obtain the thermal buckling parameters for the PZT layered cylindrical shells.

$$(\mathbf{K} + \chi\mathbf{K}_\sigma)\mathbf{x}_b = 0. \tag{18}$$

In the above equation $\mathbf{K}$ is the structural stiffness matrix, $\mathbf{K}_\sigma$ is the geometric stiffness matrix, contribution from the thermal load due to steady state axisymmetric temperature. χ are the

buckling eigenvalues which multiplies the applied temperature to give the critical buckling temperature and $\{\mathbf{x}_b\}$ is the mode shape.

Using Lagrange's equation, the equation of motion for an element is

$$\mathbf{m}_e\ddot{\mathbf{d}}_e + \mathbf{c}_{ae}\dot{\mathbf{d}}_e + (\mathbf{k}_e + \mathbf{k}_{\sigma e})\mathbf{d}_e = 0$$

and the global equation of motion for the PZT layered cylindrical shell will take the form

$$[\mathbf{M}]\{\ddot{\mathbf{d}}\} + [\mathbf{C}_d]\{\dot{\mathbf{d}}\} + [\mathbf{K} + \mathbf{K}_\sigma]\{\mathbf{d}\} = 0 \tag{19}$$

Eq. (19) is cast in the state space form which results in unsymmetric eigenvalue problem.

$$\begin{bmatrix} -\mathbf{C}_d & -\mathbf{M} \\ \mathbf{M} & 0 \end{bmatrix} \begin{Bmatrix} \mathbf{d} \\ \varpi\mathbf{d} \end{Bmatrix} = \varpi \begin{bmatrix} \mathbf{K} + \mathbf{K}_\sigma & 0 \\ 0 & \mathbf{M} \end{bmatrix} \begin{Bmatrix} \mathbf{d} \\ \varpi\mathbf{d} \end{Bmatrix}, \tag{20}$$

where ϖ is the complex eigenvalue. Eq. (20) is solved for eigenvalues and active damping ratio using LAPACK's DGEVG subroutine [35]. Let $\varpi = \varpi_R + \mathrm{i}\varpi_\mathrm{I}$, then the natural frequency will equal to ϖ_I rad/s and the active damping ratio will be equal to

$$\zeta = \frac{-\varpi_R}{\sqrt{\varpi_R^2 + \varpi_\mathrm{I}^2}}.$$

5. Validating the formulation

5.1. Validation of critical buckling temperature

Thangarathnam et al. [36] have carried out thermal buckling analysis of composite cylindrical shells under the influence of mechanical and thermal loads using semiloof finite element. Studies of the results on buckling of symmetric cross ply composite cylindrical shell under uniform temperature with simply supported boundary condition were presented. The same results are simulated using the present formulation for the same composite cylindrical shell and these are published in Ref. [24].

6. Numerical simulations—results and discussion

Free vibratory characteristics under a steady state axisymmetric temperature of a PZT-4 bonded cylindrical shell made of composite material and mild steel were studied and their results are presented in this section. The dimensions of the cylindrical shell are as follows: length of shell $l = 1.83$ m, radius of the shell $r = 0.876$ m. The thickness of the shell is 3.0 mm and thickness of PZT-4 layer is 0.02 mm. Two boundary conditions are considered in the study namely simply supported and clamped–free. The simply supported boundary condition used in the study is as follows: $u = 0, v = 0, w = 0, \psi_s \neq 0$ and $\psi_\theta \neq 0$ at the two edges of the shell, Thangaratnam [37]. The material properties used in the numerical study are listed in Table 1. The steady state temperature distribution is assumed, and all material properties are temperature independent in this study. The reference temperature, T_o, is assumed as 20°C, at which the body is free of stresses.

Table 1
Material properties, Thangaratnam [37], Saravanan [26], and Fung et al. [10]

		HS-graphite/epoxy	Mild steel	Piezoceramic (PZT4)
Young's modulus (GPa)	E_{11}	180.8	210.0	81.3
	E_{22}	10.4	210.0	81.3
	E_{33}	10.4	210.0	64.5
Shear modulus (GPa)	G_{12}	7.234	80.0	30.6
	G_{31}	7.234	80.0	25.6
	G_{23}	7.234	80.0	25.6
The Poisson ratio	ν_{12}	0.28	0.30	0.329
	ν_{13}	0.28	0.30	0.432
	ν_{23}	0.28	0.30	0.432
Density (kg/m^3)	ρ	1389.23	7860	7600
Piezoelectric properties (C/m^2)	e_{31}	—	—	5.20
	e_{32}	—	—	−5.20
Dielectric constant (C^2/(N m^2))	ξ_{33}	—	—	11505.0×10^{-12}
Coefficient of thermal expansion (per °C)	α_{11}	11.34×10^{-6}	1.1×10^{-5}	1.2×10^{-6}
	α_{22}	36.9×10^{-6}	1.1×10^{-5}	1.2×10^{-6}
Thermal stress coefficient (N/m^2 °C)	λ	1.08×10^6	1.08×10^6	1.03×10^5
Pyroelectric constant (C/m^2 °C)	P	—	—	0.25×10^{-4}
Ambient temperature (°C)	T_o	20	20	20

The buckling temperatures, T, reported in the paper are equal to difference between the absolute temperature and the stress free temperature ($T = T_{actual} - T_o$).

6.1. Convergence study

A three-node isoparametric line element is used for the finite element mesh of the cylindrical shell laminate. To start with it is necessary to carry out a convergence study as far as the number of elements required for finite element mesh in order to obtain a reasonable accuracy in the results from the finite element analysis. Two finite element meshes were chosen for the same, one with 15 elements and the other with 20 elements. Two cases are considered one for the PZT layered mild steel shell and the other for HS-graphite/epoxy with lamina angle equal to 0°. Buckling temperatures are evaluated. Table 2 lists the lowest critical buckling temperature and the corresponding mode. The convergence as far as lowest critical buckling temperature is concerned is very good. The critical buckling temperature for other modes show a reasonable convergence between 15 and 20 elements mesh design. In the present study the finite element model of the PZT layered cylindrical shell uses 15 elements, from point of view of quicker computation.

6.2. Comparative results and discussion

A detailed comparative discussion is presented on (i) the free vibration natural frequency characteristics, (ii) static thermal buckling temperatures, (iii) natural frequency variation with respect to axisymmetric temperature, and (iv) variation of active damping ratio against

Table 2
Convergence of critical buckling temperature in two finite element mesh models

Modes	Mild steel		HS-graphite/epoxy (Ply angle 0°)	
	15 elements	20 elements	15 elements	20 elements
(1,1)	239.2	210.4	70.4	68.4
(2,1)	237.7	210.3	69.9	68.0
(3,1)	235.2	209.9	69.1	67.2
(4,1)	231.9	209.5	67.9	66.2
(5,1)	228.0	208.9	66.4	64.8
(6,1)	223.6	208.3	64.6	63.2
(7,1)	219.0	207.5	62.5	61.3
(8,1)	214.3	206.5	60.1	59.2
(9,1)	209.8	205.4	57.6	56.9
(10,1)	205.4	203.9	54.9	54.5
(11,1)	201.2	202.0	52.3	52.1
(12,1)	197.2	199.5	50.3	50.2
(13,1)	193.6	196.7	49.2	49.0
(14,1)	190.9	194.0	48.7	48.6
(15,1)	189.8	192.6	48.9	48.7
(16,1)	190.5	193.1	49.5	49.3
(17,1)	193.1	195.5	50.6	50.2
(18,1)	197.4	199.6	51.9	51.6
(19,1)	203.3	205.2	53.6	53.2
(20,1)	210.6	211.9	55.6	55.1

axisymmetric temperature of the laminated shell made of two materials with simply supported and clamped–free boundary condition. Importance of the role of fiber angle in composite material is brought to light in view of thermal buckling temperature and hence its influence on free vibratory characteristics.

6.2.1. Comparison of free vibration frequencies for PZT bonded composite and mild steel cylindrical shell with simply supported boundary condition

The free vibration natural frequencies of PZT layered HS-graphite/epoxy cylindrical shell with different fiber orientations for the first axial mode associated with first twenty two harmonics are presented in Fig. 2.

On closely examining these curves the magnitude of the natural frequencies are almost close to one another for the lower harmonics. This is probably due to the membrane strain energy being more or less the same for composite cylindrical shell with different fiber orientations. The bending strain energy differs considerably for the composite shell depending on the fiber orientation. In the higher harmonics region the bending strain energy differs considerably among shells with various fiber orientation. Bending strain energy is lower for composite cylindrical shell with fiber angles 0°, 15°, 30° and 45° hence the natural frequencies are lower in magnitude. For a shell with fiber orientations 90° and 60° the natural frequencies are higher on the higher harmonic region, which

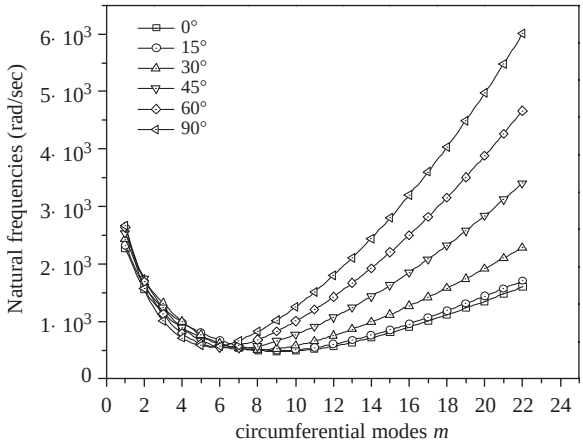

Fig. 2. First axial mode natural frequencies for PZT layered composite cylindrical shell with simply supported boundary condition.

Table 3
Lowest natural frequencies of the simply supported composite shell laminate

Fibre angle	(m,n)	Natural frequency (rad/s)
0°	(9,1)	475.6
15°	(9,1)	496.1
30°	(8,1)	502.8
45°	(7,1)	528.7
60°	(6,1)	549.4
90°	(6,1)	572.2

is apparently due to very high bending strain energy. Table 3 lists the lowest natural frequency of the composite shell with various fiber angles.

The change in the circumferential mode corresponding to lowest natural frequency of the composite shell laminate is not drastic as the fiber angle is increased. Fig. 3 shows the first axial mode natural frequency for PZT layered mild steel shell associated with first 22 circumferential modes.

The lowest natural frequency occurs for mode (8,1) and is 556.6 rad/s. It is seen from Table 3 that the frequencies of composite shell are lower than that of mild steel shell for some fiber angles. In contrast at some fiber angles the frequencies are comparable to that of mild steel.

6.2.2. Comparison of free vibration natural frequencies for PZT bonded composite and mild steel cylindrical shell for clamped–free boundary condition

Fig. 4 shows the first axial mode natural frequencies associated with first 20 circumferential modes of PZT layered composite shell with clamped–free boundary condition.

In contrast to the composite shell with simply supported boundary condition it is seen here that the membrane strain energy differs in magnitude for lower number of circumferential harmonics depending on the fiber angle. For higher circumferential number the bending strain energy is low

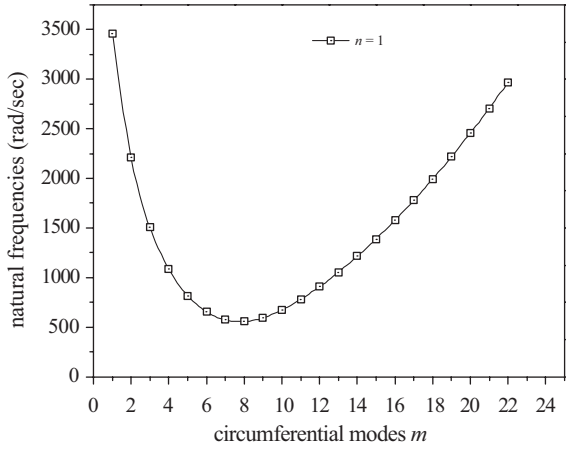

Fig. 3. First axial mode natural frequencies for PZT layered mild steel cylindrical shell with simply supported boundary condition.

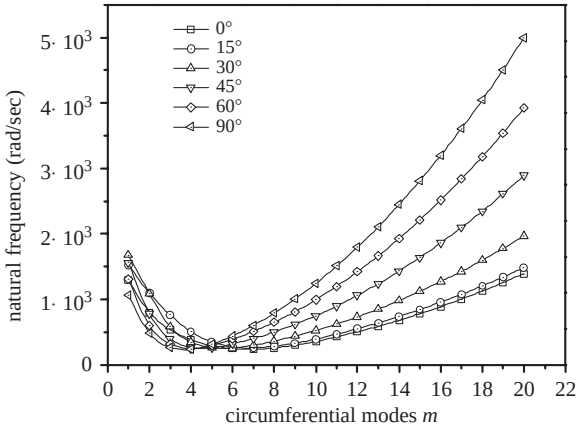

Fig. 4. First axial mode natural frequencies for PZT layered composite cylindrical shell with clamped–free boundary condition.

in case of fiber angles 0°, 15°, 30° and 45° where as it is higher for fiber angles 60° and 90° for higher number of harmonics. The magnitude of the lowest natural frequency and the corresponding mode are listed in Table 4. In general the behavior is similar to that of simply supported shells. As expected the frequencies of clamped–free shell are lower than that of simply supported shell.

Fig. 5 shows the typical variation of the frequency characteristic for clamped–free PZT bonded mild steel cylindrical shell. The lowest natural frequency in the first mode is associated with fifth circumferential mode and its magnitude is 230.6 rad/s. The comparative trend in the frequencies between composite and mild steel clamped–free shell is more or less the same as that of simply supported shell.

Table 4
Lowest natural frequencies for clamped-free PZT layered composite shell

Fibre angle	Modes	Natural frequency (rad/s)
0°	(7,1)	237.3
15°	(7,1)	257.4
30°	(6,1)	253.2
45°	(5,1)	258.7
60°	(4,1)	249.7
90°	(4,1)	236.3

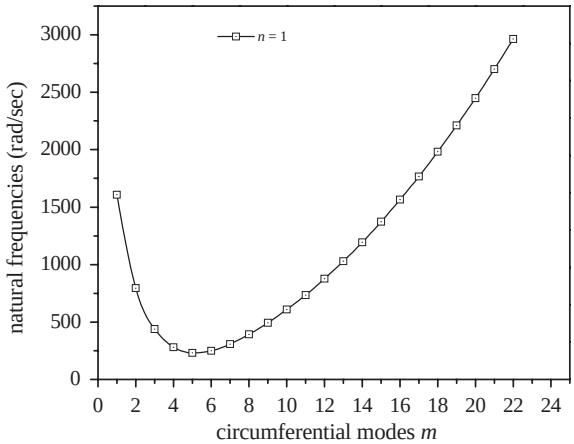

Fig. 5. First axial mode natural frequencies of PZT layered mild steel shell with clamped–free boundary condition.

6.2.3. *Comparison of critical thermal buckling temperature of simply supported composite and mild steel cylindrical shell*

Static thermal buckling analysis is required in order to determine the critical thermal buckling temperatures. This will be highly useful when studying the frequency characteristics and active damping ratio with respect to temperature. Table 5 lists the first axial mode (lowest) critical buckling temperatures for PZT bonded graphite/epoxy composite shell with $l/r = 2.08$ and simply supported boundary condition. Composite shells with various fiber angles are considered in the study.

From the table it is seen that the critical buckling temperatures are highly dependent on the fiber angle and circumferential mode. It is as low as 37.6°C for 15° fiber angle and as high as 357.9°C for 60° fiber angle as far as the lowest critical thermal buckling temperature is concerned. While studying the free vibratory characteristics, depending upon the fiber angle and circumferential mode, the upper limit of the operating temperature was limited at 0.98 times the critical buckling temperature. Under practical circumstances for active controlled systems using piezoceramic materials Curie temperatures should also be borne in mind. For PZT-4 the Curie temperature is 300°C. However, in this numerical study the consequence of Curie temperature has been ignored. In addition the critical buckling temperatures of mild steel shell has

Table 5
Lowest thermal buckling temperatures for simply supported PZT bonded composite shell and mild steel shell

Modes	Fibre angle of shell lamina						Mild steel
	0°	15°	30°	45°	60°	90°	
	Critical buckling temperatures						
(1,1)	70.4	46.7	55.2	140.0	474.8	1085.0	219.2
(2,1)	69.9	46.6	55.4	140.7	463.2	966.3	217.7
(3,1)	69.1	46.4	55.6	141.6	449.6	817.8	215.2
(4,1)	67.9	46.0	55.7	142.8	435.7	671.9	211.9
(5,1)	66.4	45.5	55.7	144.5	422.2	453.8	208.0
(6,1)	64.6	44.8	55.7	146.6	408.9	362.5	203.6
(7,1)	62.5	44.1	55.5	149.3	395.3	301.0	199.0
(8,1)	60.1	43.2	54.2	152.3	381.6	265.4	194.3
(9,1)	57.6	42.0	51.7	155.6	369.3	232.0	189.8
(10,1)	54.9	39.5	50.4	156.8	360.8	207.5	185.4
(11,1)	52.3	38.5	50.8	160.8	357.9	191.7	181.2
(12,1)	50.3	38.1	50.9	165.6	361.4	182.6	177.2
(13,1)	49.2	37.6	52.9	173.0	371.1	178.4	173.6
(14,1)	48.7	38.2	54.9	182.1	386.4	178.4	170.9
(15,1)	48.9	39.1	51.1	189.1	406.5	182.4	169.8
(16,1)	49.5	40.0	51.1	189.1	430.9	190.2	170.5
(17,1)	50.6	41.3	52.8	189.5	458.7	201.7	173.1
(18,1)	51.9	42.5	54.9	196.1	489.1	216.9	177.4
(19,1)	53.6	42.1	57.3	207.5	521.8	235.9	183.3
(20,1)	55.6	41.5	60.0	222.0	557.1	258.6	190.6
(21,1)	57.8	42.2	63.1	239.2	595.6	284.9	199.4
(22,1)	60.2	43.4	66.3	258.7	637.8	314.9	209.6

also been reported in Table 5. Even though, in general, mild steel shell has better thermal buckling characteristics compared to composite shell, for most of the fiber orientation it is found that the buckling characteristics of 60° fiber angle composite is superior compared to mild steel. In the section which deals with frequency characteristics of shells under thermal environment an attempt is made to explain as to why the thermal buckling temperature differs in composite shells with various fiber angles on the basis of initial thermal stress distribution in the cylindrical shells.

6.2.4. Comparison of critical thermal buckling temperatures of clamped–free PZT layered composite and mild steel cylindrical shell

Table 6 lists the lowest buckling temperatures for a clamped–free composite shell laminate. Since one end of the shell laminate is free to expand the initial stresses will be lower compared to the shell laminate with simply supported ends. Hence one can expect very large magnitude of the critical buckling temperature. As noticed from Table 6 the lowest critical buckling temperatures are high in magnitude when compared to composite shell laminate with simply supported ends. The critical buckling temperatures are extremely high especially for composite laminate with fiber angles 45°, 30°, 15°, and 0°. At this point it is interesting to note that for the same fiber angles the cylindrical shell laminate with simply supported boundary condition possess extremely low

Table 6
Lowest thermal buckling temperatures for clamped–free PZT bonded HS-graphite/epoxy shell and mild steel shell

Modes	Fibre angle of shell lamina						Mild steel
	0°	15°	30°	45°	60°	90°	
	Critical buckling temperatures						
(1,1)	89475.2	31919.3	22600.0	15299.0	12148.9	389827.6	93570.9
(2,1)	55256.0	28274.4	21703.1	15027.0	12481.9	86914.9	93624.6
(3,1)	29592.3	22572.6	20335.7	14813.7	11784.8	18793.6	79555.3
(4,1)	16659.4	16546.4	18517.2	14357.0	5843.9	6500.3	35362.0
(5,1)	10174.4	11768.7	16364.7	13305.9	2824.9	2874.0	16612.4
(6,1)	6679.4	8462.7	14114.9	10412.1	1599.9	1514.8	9071.6
(7,1)	5167.0	6255.5	12001.8	6662.7	1024.3	918.4	5467.1
(8,1)	5142.1	4770.2	17694.2	4672.4	724.2	625.8	3590.2
(9,1)	2228.1	3826.2	7296.2	3528.3	557.8	472.5	2538.4
(10,1)	1676.9	4032.6	5663.5	2851.9	462.6	389.8	1910.5
(11,1)	1392.3	7559.2	4687.2	2445.5	408.0	346.2	1520.5
(12,1)	1408.2	6114.4	4073.6	2201.8	377.9	326.1	1272.6
(13,1)	6329.5	2436.2	3692.3	2060.0	363.4	320.9	1113.5
(14,1)	1040.1	1651.9	3463.2	1984.2	359.1	325.8	1012.5
(15,1)	883.7	1435.8	3341.9	1952.4	361.8	337.5	951.0
(16,1)	794.5	1303.7	3490.3	1950.6	369.4	354.1	917.5
(17,1)	725.8	1201.5	16686.0	1969.8	380.3	374.1	904.1
(18,1)	672.2	1120.7	3520.2	2004.0	393.8	396.7	905.6
(19,1)	630.2	1056.4	3290.1	2048.4	409.1	421.2	918.4
(20,1)	597.1	1005.0	3135.9	2101.1	425.7	447.2	939.8

thermal buckling temperatures. Further for clamped–free cylindrical shell laminate, the critical buckling temperatures are comparatively lower for higher harmonics (from eighth harmonic) in case of composite shells with fiber angles 60° and 90°.

Table 6 also lists the thermal buckling temperatures for mild steel cylindrical shell for the first 20 circumferential modes. Here again the thermal buckling temperatures are extremely high. Under normal safe operating temperature it is clear that the question of thermal buckling may not be of a serious concern either in the case of orthotropic or isotropic cylindrical shell with clamped–free boundary condition. As stated in the previous section the reasons for high thermal buckling temperatures and the role of fiber angle can be explained by studying the nature of distribution of the initial stresses due to a thermal loading in the clamped–free cylindrical shell laminate.

A keen observation of the critical thermal buckling temperatures listed in Tables 5 and 6 clearly brings out the fact that not only the fiber angle plays a vital role in attributing the limit to thermal buckling temperatures, but also the structural boundary condition has a major role in deciding on the thermal buckling temperatures.

6.2.5. Influence of axisymmetric temperature on the natural frequency

6.2.5.1. PZT bonded composite and mild steel cylindrical shell with $l/r = 2.08$ *and simply supported boundary condition*. The nature of variation of the first axial mode natural frequency of the

piezoelectric laminated composite shell is evaluated for various axisymmetric temperatures. Operating temperature spans from ambient temperature to a temperature magnitude of 0.98 times the critical buckling temperature of various circumferential modes. Fig. 6 illustrates the frequency characteristics of the composite shell laminate for different fiber orientation. For each composite shell laminate the variations are studied for different circumferential modes viz. 1, 5, 10 and 15. In

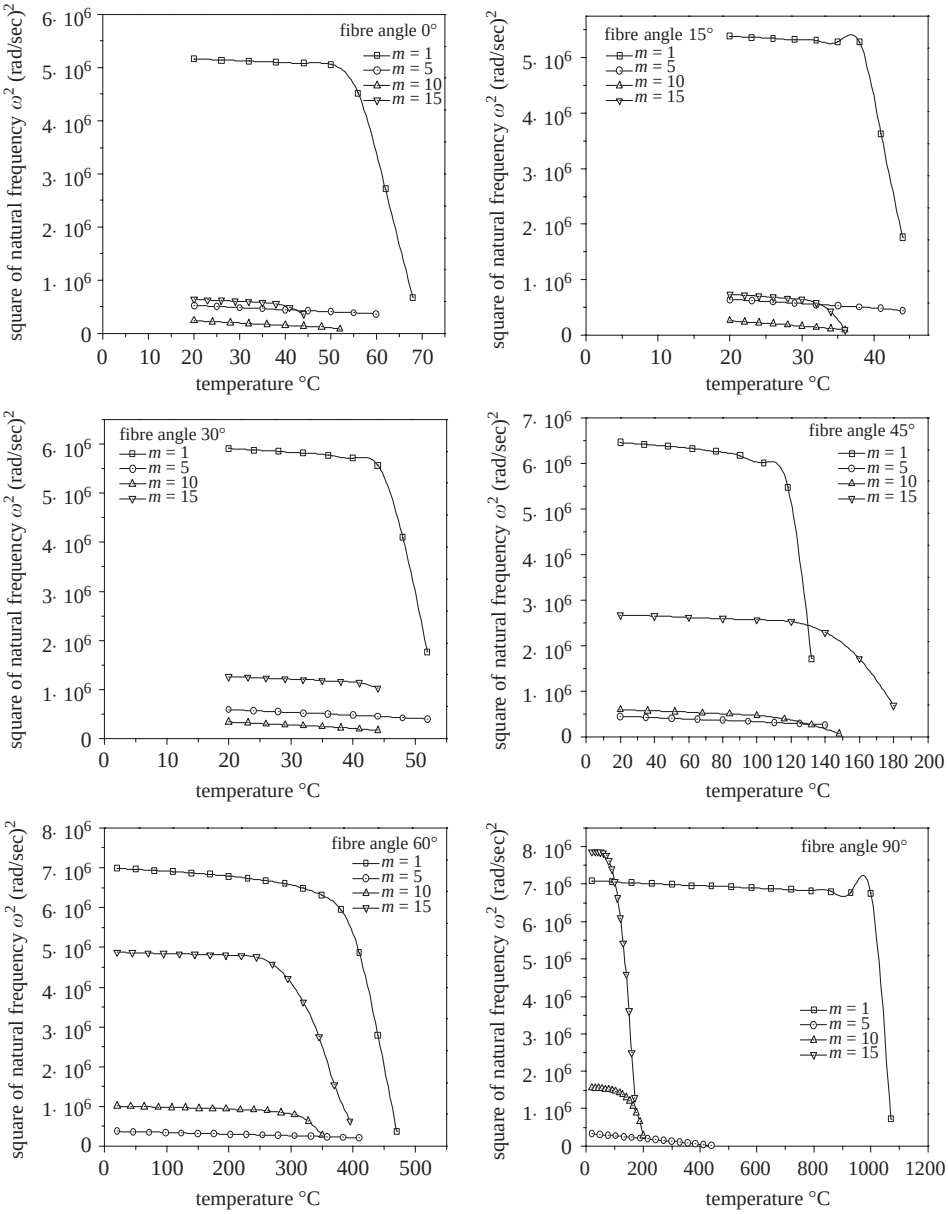

Fig. 6. Variation of the square of the lowest natural frequency versus axisymmetric temperature for a simply supported HS-graphite/epoxy cylindrical shell bonded with PZT sensors/actuators.

each of the cases as expected the natural frequency reduces as the temperature of the shell laminate increases. The fall in natural frequency is minimal for the initial rise in temperature. This trend is true in case of all composite shell laminates irrespective of the fiber angle and mode. Further, consider mode (1,1), it is seen that as the temperature is increased and reaches a reasonably high temperature compared to thermal buckling temperature there is a sudden drop in the magnitude of the frequency. This trend continues and it tends to zero as the temperature is further increased to a magnitude close to the critical buckling temperature. This behavior in the variation of natural frequency may probably be due to high magnitude of initial stresses near about the buckling temperature.

This trend is well observed for the composite shell irrespective of the fiber angle considered in the study. For mode (5,1) the variation of the frequency with respect to temperature is almost linear up to critical buckling temperature (this is clearly seen in Fig. 6 for a composite shell with 90° fiber orientation) irrespective of fiber angle. The variation of natural frequency with respect to temperature follows a linear path for mode (10,1) for composite shell with fiber angles 0°, 15°, and 30°. But in case of composite shell with fiber angles 45°, 60°, and 90° the nature of variation is initially linear with minimal reduction in frequency as temperature increases. Further for higher temperatures (more or less close to thermal buckling temperatures) the frequency reduces appreciably as seen for shell with 90° fiber angle. The nature of variation in the natural frequency in mode (15,1) is more or less similar to that observed in mode (1,1), excepting that the steepness of the fall in frequency at higher temperatures is less. Thus it is clear that the trend in variation of the natural frequency with respect to temperature differs from mode to mode.

Under ambient conditions the frequency characteristics as depicted in Figs. 2 and 3 indicate that the magnitudes of the natural frequencies do not differ much for modes from (1,1) to (8,1) for the composite shell with various fiber angles considered. Beyond these modes there is appreciable difference in frequencies. Again in this region the exception are among composite shells with fiber angles 0°, 15° and 90°. But in contrast the natural frequency characteristics differ considerably for composite shells depending on the fiber angle when operating in steady state isothermal conditions. The permissible range of operating temperature is very small for composite shells with fiber angles 0°, 15° and 30° when compared to composite shells with fiber angles 45°, 60° and 90°.

In order to explain the behavior of variation of natural frequency with respect to temperature for different fiber orientations an attempt was made to study the distribution of the initial stress resultants due to thermal loading. Fig. 7 shows the distribution of the axial stress resultants along the length of the shell laminate for various fiber angles. The axial stress resultants (i.e. compressive in nature) are the highest for shell with fiber angle 15°. The stress resultants for composite shell with fiber angles 30° and 0° are less compared to 15° but are on higher side when compared to shell with fiber angles 45°, 60° and 90°. Composite shells with fiber angles 45°, 90° and 60° have comparatively very low magnitudes of stress resultants, respectively. The nature of distribution and magnitude of the initial stress resultants to some extent governs the limit on the critical thermal buckling temperature.

Looking back at critical buckling temperatures in Table 5, accordingly the critical thermal buckling temperatures are very high in case of composite shell tailored with fiber angles 45°, 60° and 90°. Composite shell with 15° fiber angle should have the lowest magnitude of critical thermal buckling temperatures. Hence it is concluded that the geometric stiffness matrix (which depends

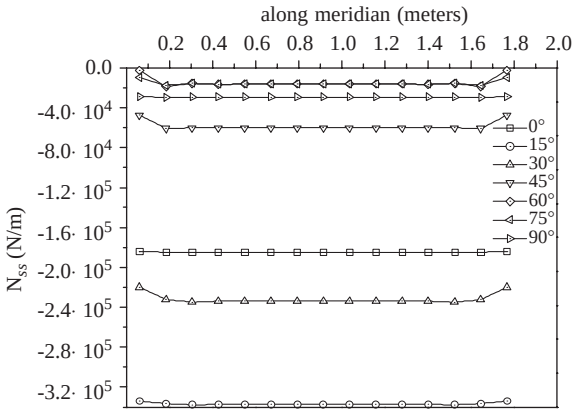

Fig. 7. Distribution of axial stress resultants N_{ss} along meridian of the composite shell laminated for various fiber angles with simply supported boundary condition.

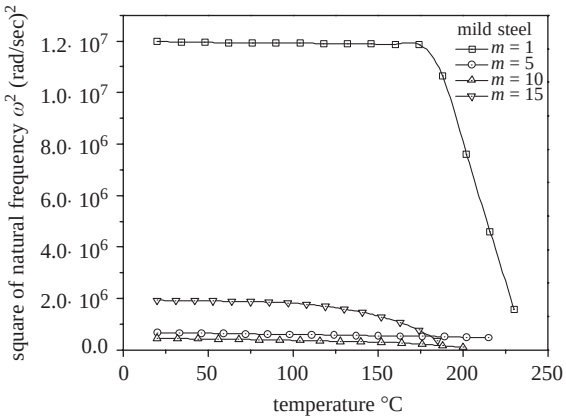

Fig. 8. Variation of the square of the natural frequency versus axisymmetric temperature for PZT layered mild steel shell with simply supported boundary condition.

on the initial stresses of the system) plays a vital role in deciding the frequency characteristics of the composite shell under steady state isothermal conditions.

For isotropic material like mild steel considered in the study, the variation of the natural frequency with respect to axisymmetric temperature are found for few modes namely (1,1), (5,1), (10,1) and (15,1) and these are illustrated in Fig. 8.

The trend in the variation of natural frequency with respect to temperature is similar to those for composite shell with fiber angles 0°, 15° and 30°. One of the reasons for the same trend can be attributed to the similar nature of the free vibration characteristics of the mild steel shell laminate when compared to composite shell laminate with fiber angles 0°, 15° and 30°.

6.2.5.2. PZT bonded composite and mild steel cylindrical shell with $l/r = 2.08$ and clamped–free boundary condition. The studies of the variation of natural frequency with respect to axisymmetric

temperature are limited to composite shell with 60° and 90° fiber angles and also to the higher circumferential harmonics like 10, 15 and 20. These results are shown in Fig. 9.

The study was conducted up to 98% of the critical buckling temperature. The plots indicate that the decrease in natural frequency is very less with increase in temperature for modes (10,1) and (15,1). Studies here too reveal that the nature of decrease in the magnitude of the natural frequency with respect to temperature increase is highly dependent on the mode and fiber angle.

Fig. 10 show the distribution of the axial stress resultants in a clamped–free PZT bonded HS-Graphite/Epoxy cylindrical shell. As expected the stress resultants are very large near the clamped edge and almost zero at the free end of the shell. The magnitude of the axial stress resultants is highest for composite with 60° fiber angle. From Fig. 10b, the stress resultants in the circumferential direction are highest for 60° and 90° fiber orientations. These facts can probably be attributed to low magnitudes of thermal buckling temperatures for higher harmonics in a clamped–free shell.

Since the critical thermal buckling temperatures are very high for clamped–free mild steel shell (refer to Table 6) based on the trends in composite shells here also one can expect the reduction in frequency with variations in the axisymmetric temperature will be very small.

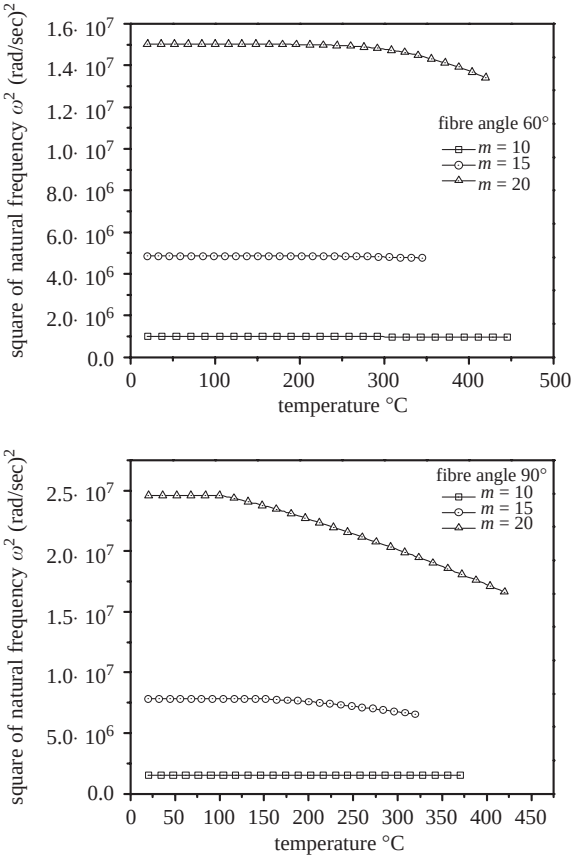

Fig. 9. Variation of the square of the lowest natural frequency versus axisymmetric temperature for clamped–free PZT layered HS-graphite/epoxy cylindrical shell.

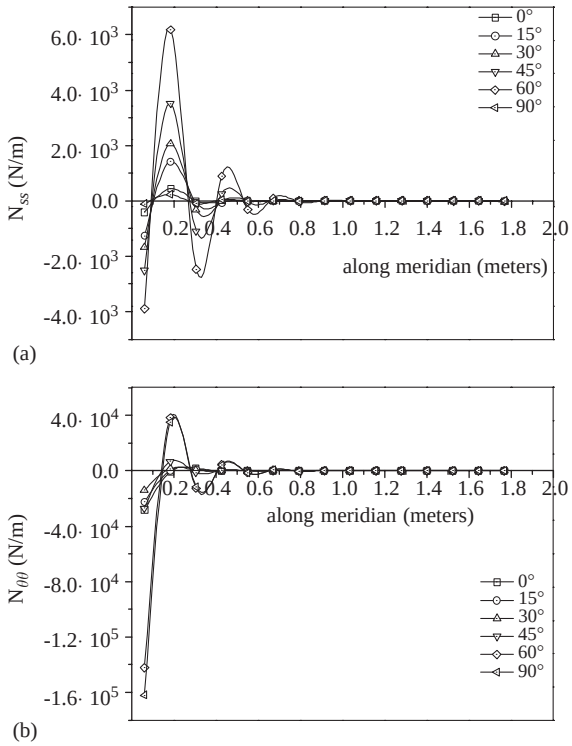

Fig. 10. Distribution of axial stress resultants (a) and circumferential stress resultants (b) along the meridian of HS-graphite/epoxy cylindrical shell bonded with PZT layer with clamped–free boundary condition.

6.3. *Influence of axisymmetric temperature on active damping ratio*

Active damping ratios are evaluated using the LAPACK's DGEVG routine. It is required to understand the nature of variation in the magnitude of the active damping ratios for various axisymmetric temperatures. Typical results have been presented for simply supported PZT bonded HS-graphite/epoxy composite shell with 60° fiber orientation and for PZT bonded mild steel cylindrical shell. Figs. 11 and 12 illustrate these results. The active damping ratios illustrated are for the first axial mode associated with circumferential modes m equal to 1,5,10 and 15. In general it is observed that depending on the mode (m, n) either system has positive active damping ratio or negative active damping ratio irrespective of the temperature changes. Accordingly the system under active control using cosine shaped PZT sensor/actuator will be stable or unstable. It is seen that for modes (1,1) and (5,1) the system is stable for most of the operating temperatures but near the buckling temperature the active damping ratio decreases drastically leading the system to become unstable.

It interesting to note that for mode (5,1) in case of PZT bonded HS-Graphite/Epoxy cylindrical shell the active damping ratio increases slightly as the operating temperature increases.

Fig. 13 shows the typical results on the variation of active damping ratios with respect to temperature for a PZT bonded HS-graphite/epoxy cylindrical shell with clamped-free boundary

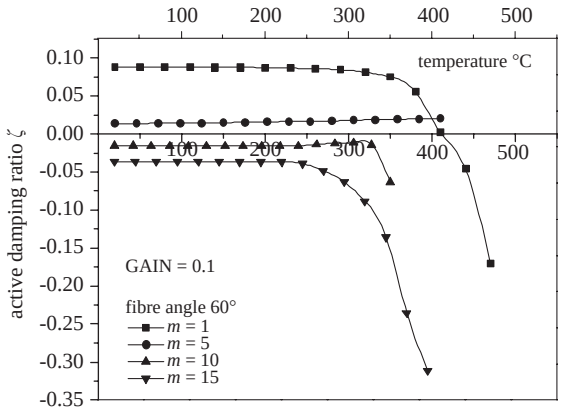

Fig. 11. Variation of the active damping ratio for first axial mode with respect axisymmetric temperature for PZT bonded HS-graphite/epoxy cylindrical shell with simply supported boundary condition.

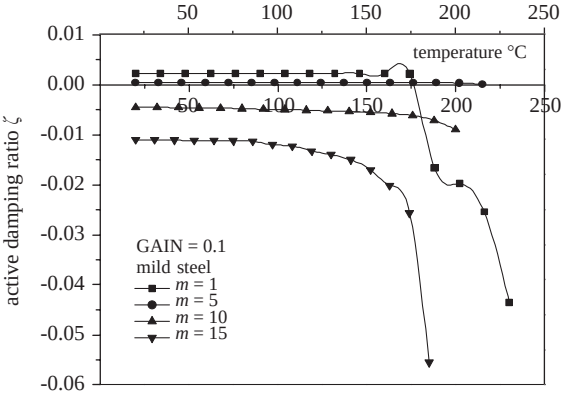

Fig. 12. Variation of active damping ratio for the first axial mode with respect to axisymmetric temperature in a PZT bonded mild steel shell with simply supported boundary condition.

condition. The active damping ratios are negative for the modes considered for study namely (10,1), (15,1) and (20,1).

For the geometry details of the cylindrical shell considered for study here the active control of vibrations at higher modes especially (10,1), (15,1) and (20,1) produce negative damping. From the above study it is clear that the magnitude of active damping ratio depends on the mode (m, n). The variation in magnitude of active damping ratio with respect to temperature is negligible when compared to active damping ratio at room temperature. This is true irrespective of the boundary condition.

7. Closure

A comparative study of the free vibratory characteristics has been presented between PZT bonded cylindrical shell made of HS-graphite/epoxy and mild steel. Simply supported and

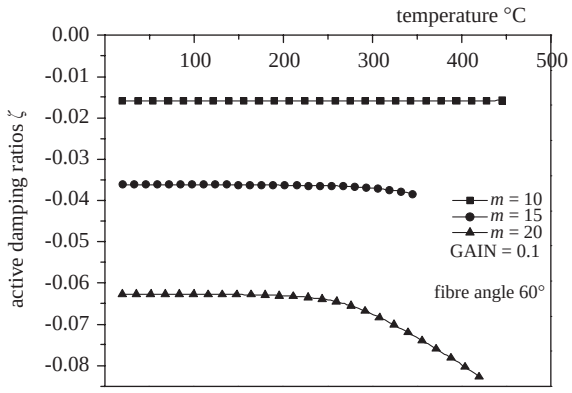

Fig. 13. Variation of active damping ratio for the first axial mode with respect to axisymmetric temperature for clamped–free PZT bonded HS-graphite/epoxy cylindrical shell.

clamped–free cylindrical shell with l/r 2.08 are considered for the study. Semi-analytical finite element formulation for the study of free vibratory characteristics of PZT bonded cylindrical shell operating in steady state isothermal conditions is discussed. The finite element code is verified by comparing the thermal buckling temperatures for composite shell laminate available in literature.

The free vibration natural frequency characteristics of PZT bonded mild steel shell shows variation similar to PZT bonded HS-graphite/epoxy cylindrical shell with fiber angle 30° in the case of simply supported boundary condition. For a clamped–free PZT bonded mild steel cylindrical shell the frequency characteristics are more or less similar to PZT bonded HS-Graphite/Epoxy cylindrical shell with 45° and 60° fiber orientation.

The thermal buckling temperatures of PZT bonded HS-Graphite/Epoxy cylindrical shells with fiber angles 60° and 90° have better thermal buckling temperatures when compared to that of mild steel shell with simply supported boundary condition. The thermal buckling temperatures of composite shell with 0°, 15°, 30°, and 45° fiber orientations are much less compared to mild steel. The lowest thermal buckling temperature in case of cylindrical shell with 15° fiber orientation is as low as 37°C compared to 358°C for 60° fiber orientation. This large difference in the thermal buckling temperature among the composite shells with different fiber orientation has been explained on the basis of initial stress resultants and it has been proved that depending on the fiber orientation one factor that governs the thermal buckling temperature is the magnitude and distribution of initial stress resultants.

The thermal buckling temperatures are high for mild steel shell as well as composite shells with clamped–free boundary condition. The influence of fiber orientation on the thermal buckling behavior of clamped–free shells is different compared to that of simply supported composite shells. It is found that the shell lamina with 30°, 45°, 15° and 0° fiber orientations have extremely higher thermal buckling temperature. This has been explained on the basis of distribution of initial stress resultants.

Free vibratory natural frequency behavior of simply supported PZT bonded HS-Graphite/Epoxy shell under thermal environment has been studied for different fiber orientations. The influence of temperature on the natural frequency of the PZT bonded cylindrical shells show that for the initial increase in the magnitude of temperature the change in the magnitude of the natural

frequency is minimal. At higher temperatures close to buckling temperature the natural frequency decreases either drastically or gradually depending on the mode. The permissible temperature also depends on the circumferential mode. Even though the free vibration characteristics of composite shell laminates at room temperature does not differ considerably especially at low circumferential mode, their characteristics differ widely under axisymmetric temperature conditions. It is found that the permissible range of temperature for the operation of the PZT bonded cylindrical shell with different fiber orientation widely differs. For example shell with 15° fiber orientation can operate up to 37°C which is very low when compared to shell with 60° fiber orientation which can operate up to 358°C. Hence the fiber angle of composite shell can be tailored to suit the temperature requirement.

Even though the variation of frequencies of clamped–free shells show a trend similar to that of simply supported shells the influence of fiber orientation on the thermal buckling temperature does not follow the same trends.

The magnitude of the active damping ratios do not vary much at various temperatures compared to the active damping ratio at room temperature until near about the buckling temperature. The active damping ratio decreases drastically as the temperature nears the thermal buckling temperature. Depending on the mode the active damping ratios are either positive or negative. From the nature of the damping it is possible to ascertain the stability of the PZT bonded shell.

References

[1] T.R. Tauchert, F. Ashida, N. Noda, S. Adali, V. Verijenko, Developments in thermopiezoelasticity with relevenace to smart composite structures, Composite Structures 48 (2000) 31–38.
[2] S.S. Rao, M. Sunar, Piezoeletricity and its use in disturbance sensing and control of flexible structures: a survey, American Society of Mechanical Engineers Applied Mechanics Review 47 (1994) 113–123.
[3] S.S. Rao, M. Sunar, Analysis of distributed thermopiezoelctric sensors and actuators in advanced intelligent structures, American Institute of Aeronautics and Astronautics Journal 31 (1993) 1280–1286.
[4] Chang-Qing Chen, YA.-Peng Shen, Piezothermoelasticity analysis for a circular cylindrical shell under the state of axisymmetric deformation, International Journal of Engineering Science 34 (1996) 1585–1600.
[5] K. Xu, A.K. Noor, Three-dimensional analytical solutions for coupled thermoelectroelastic response of multilayered cylindrical shells, American Institute of Aeronautics and Astronautics Journal 34 (1996) 802–812.
[6] S. Kapuria, P.C. Dumir, S. Sengupta, Exact piezothermoelastic axisymmetric solutions of a finite transversely isotropic cylindrical shell, Computers and Structures 61 (1996) 1085–1099.
[7] S. Kapuria, P.C. Dumir, S. Sengupta, An exact axisymmetric solution for a simply supported piezoelectric cylindrical shell, Archive of Applied Mechanics 67 (1997) 260–273.
[8] S. Kapuria, S. Sengupta, P.C. Dumir, Three-dimensional solution for a hybrid cylindrical shell under axisymmetric thermoelectric load, Archive of Applied Mechanics 67 (1997) 320–330.
[9] S. Kapuria, P.C. Dumir, S. Sengupta, Three-dimensional solution for a hybrid cylindrical shell under axisymmetric thermoelectric load, American Institute of Aeronautics and Astronautics Journal 35 (11) (1997) 1792–1795.
[10] Rong-Fong Fung, Jeng-Sheng Huang, Shang-Chin Jan, Dynamic analysis of a piezothermoelastic resonator with various shapes, American Society of Mechanical Engineers Journal of Vibration and Acoustics 122 (2000) 244–253.
[11] H.S. Tzou, Y. Bao, A theory on anisotropic piezothermoelastic shell laminates with sensor/actuator applications, Journal of Sound and Vibration 184 (1995) 453–473.
[12] H.S. Tzou, R.V. Howard, A piezothermoelastic thin shell theory applied to active structures, American Society of Mechanical Engineers Journal of Vibration and Acoustics 116 (1994) 295–302.

[13] H.S. Tzou, R. Ye, Piezothermoelasticity and precision control of piezoelectric systems: theory and finite element analysis, American Society of Mechanical Engineers Journal of Vibration and Acoustics 116 (1994) 489–495.

[14] H.S. Tzou, Y. Bao, Nonlinear piezothermoelasticity and multi-field actuations, Part I: nonlinear anisotropic piezothermoelastic shell laminates, American Society of Mechanical Engineers Journal of Vibration and Acoustics 119 (1997) 371–381.

[15] H.S. Tzou, Y.H. Zhou, Nonlinear piezothermoelasticity and multi-field actuations, Part 2: control of nonlinear deflection, buckling and dynamics, American Society of Mechanical Engineers Journal of Vibration and Acoustics 119 (1997) 382–389.

[16] Ho-Jun Lee, D.A. Saravanos, Amixed multi-field finite element formulation for thermopiezoelectric composite shells, International Journal of Solids and Structures 37 (2000) 4949–4967.

[17] H. Gu, A. Chattopadhyay, J. Li, X. Zhou, A higher order temperature theory for coupled thermo piezoelectric-mechanical modeling of smart structures, International Journal of Solids and Structures 37 (2000) 6479–6497.

[18] X.Q. He, T.Y. Ng, S. Sivashanker, K.M. Liew, Active control of FGM plates with integrated piezoelectric sensors and actuators, International Journal of Solids and Structures 38 (2001) 1641–1655.

[19] K.M. Liew, X.Q. He, T.Y. Ng, S. Sivashanker, Active control of FGM plates subjected to a temperature gradient: modelling via finite element method based on FSDT, International Journal for Numerical Methods in Engineering 52 (2001) 1253–1271.

[20] X.Q. He, K.M. Liew, T.Y. Ng, S. Sivashanker, A FEM model for the active control of curved FGM shells using piezoelectric sensor/actuator layers, International Journal for Numerical Methods in Engineering 54 (2002) 853–870.

[21] T.Y. Ng, K.Y. Lam, K.M. Liew, Effects of FGM materials on the parametric resonance of plate structures, Computer Methods in Applied Mechanics and Engineering 190 (2000) 953–962.

[22] T.Y. Ng, K.Y. Lam, K.M. Liew, J.N. Reddy, Dynamic stability analysis of functionally graded cylindrical shells under periodic axial loading, International Journal of Solids and Structures 38 (2001) 1259–1309.

[23] T.Y. Ng, X.Q. He, K.M. Liew, Finite element modeling of active control of functionally graded shells in frequency domain via piezoelectric sensors and actuators, Computational Mechanics 28 (2002) 1–9.

[24] N. Ganesan, R. Kadoli, Buckling and dynamic analysis of piezothermoelastic composite cylindrical shell, Composite Structures 59 (2003) 45–60.

[25] S.R. Rao, N. Ganesan, Interlaminar stresses in shells of revolution, Mechanics of Composite Materials and Structures 3 (1996) 321–339.

[26] C. Saravanan, N. Ganesan, V. Ramamurti, Semianalytical finite element analysis of active damping in smart cylindrical shells, American Society of Mechanical Engineers Journal of Vibration and Control 6 (2000) 849–873.

[27] H.S. Tzou, J.P. Zhong, M. Natori, Sensor mechanics of distributed shell convolving sensors applied to flexible rings, American Society of Mechanical Engineers Journal of Vibration and Acoustics 115 (1993) 40–46.

[28] R.D. Mindlin, Equations of high frequency vibrations of thermopiezoelectric crystal plates, International Journal of Solids and Structures 10 (1974) 625–637.

[29] K.M. Liew, Vibration of shallow shells: a review with bibliography, American Society of Mechanical Engineers Applied Mechanics Review 50 8 (1997) 431–444.

[30] S.R. Rao, Static and Dynamic Problems in Laminated Beams and Axisymmetric Shells, Ph.D. Thesis, Indian Institute of Technology Madras, India, 1997.

[31] R.D. Cook, D.S. Malkus, M.E. Plesha, Concepts and Applications of Finite Element Analysis, John Wiley and Sons, Singapore, 2000.

[32] H.S. Tzou, Distributed modal identifications and vibrations control of continua: theory and applications, American Society of Mechanical Engineers Journal of Dynamic systems, Measurements and Control 113 (1991) 494–499.

[33] H.S. Tzou, C.I. Tseng, Distributed modal identification and vibration control of continua: piezoelectric finite element formulation and analysis, American Society of Mechanical Engineers Journal of Dynamic systems, Measurements, and Control 113 (1991) 500–505.

[34] H.S. Tzou, Piezoelectric Shells Distributed Sensing and Control of Continua, Kluwer Academic Publishers, Dordrecht, The Netherlands, 1993.
[35] G.H. Golub, C.F. Van Loan, Matrix Computation, 3rd Edition, Johns Hopkins University Press, Baltimore, 1996.
[36] R.K. Thangaratnam, J. Palaninathan, Ramachandran, Buckling of composite cylindrical shells, Journal of Aero Society of India 41 (1989) 47–54.
[37] R.K. Thangaratnam, Thermal buckling of laminated composite plates and shells, Ph. D. Thesis, Indian Institute of Technology Madras, India, 1989.